

# CT Image Enhancement Using Stacked Generative Adversarial Networks and Transfer Learning for Lesion Segmentation Improvement

Youbao Tang<sup>1\*</sup>, Jinzheng Cai<sup>1,2\*</sup>, Le Lu<sup>1</sup>, Adam P. Harrison<sup>1</sup>, Ke Yan<sup>1</sup>,  
Jing Xiao<sup>3</sup>, Lin Yang<sup>2</sup>, Ronald M. Summers<sup>1</sup>

<sup>1</sup> National Institutes of Health Clinical Center, Bethesda, MD 20892, USA  
youbao.tang@nih.gov

<sup>2</sup> University of Florida, Gainesville, FL 32611, USA

<sup>3</sup> Ping An Insurance Company of China, Shenzhen, 510852, China

**Abstract.** Automated lesion segmentation from computed tomography (CT) is an important and challenging task in medical image analysis. While many advancements have been made, there is room for continued improvements. One hurdle is that CT images can exhibit high noise and low contrast, particularly in lower dosages. To address this, we focus on a preprocessing method for CT images that uses stacked generative adversarial networks (SGAN) approach. The first GAN reduces the noise in the CT image and the second GAN generates a higher resolution image with enhanced boundaries and high contrast. To make up for the absence of high quality CT images, we detail how to synthesize a large number of low- and high-quality natural images and use transfer learning with progressively larger amounts of CT images. We apply both the classic GrabCut method and the modern holistically nested network (HNN) to lesion segmentation, testing whether SGAN can yield improved lesion segmentation. Experimental results on the DeepLesion dataset demonstrate that the SGAN enhancements alone can push GrabCut performance over HNN trained on original images. We also demonstrate that HNN + SGAN performs best compared against four other enhancement methods, including when using only a single GAN.

**Keywords:** CT image enhancement, lesion segmentation, stacked generative adversarial networks, transfer learning

## 1 Introduction

There are many useful and important applications in medical image analysis, *e.g.*, measurement estimation [1], lung segmentation [2], lesion segmentation [3], etc. Accurate lesion segmentation from computed tomography (CT) scans plays a crucial role in computer aided diagnosis (CAD) tasks, *e.g.*, quantitative disease progression, tumor growth evaluation after treatment, pathology detection

---

\* indicates equal contribution

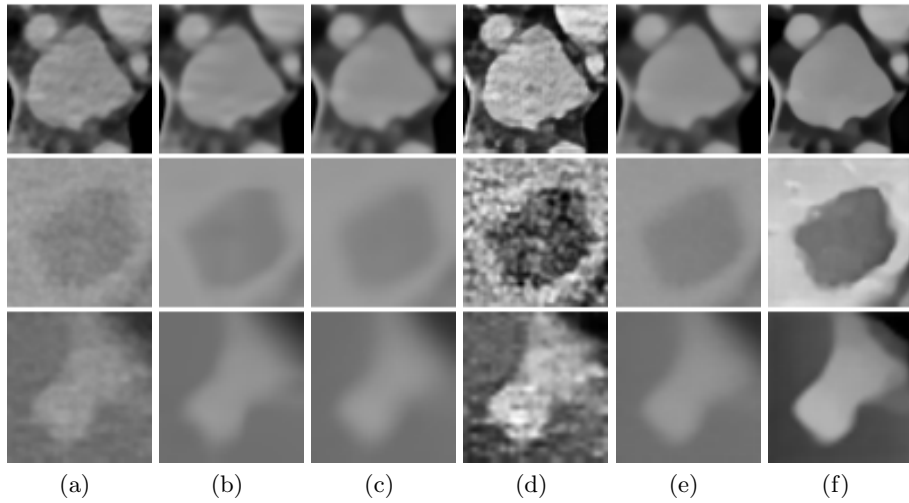


**Fig. 1.** Three examples of CT image enhancement results using different methods on original images (a), BM3D (b), DnCNN (c), single GAN (d), our denoising GAN (e), and our SGAN (f).

and surgical assistance. Quantitative analysis of tumor extents could provide valuable information for treatment planning. Manual lesion segmentation is highly tedious and time consuming, motivating a number of works on automatic lesion segmentation [3–5]. However, as more and more elaborately designed segmentation methods are proposed, performance improvement may plateau. In particular, CT images are often noisy and suffer from low contrast due to radiation dosage limits, as shown in the first row of Fig. 1. The collection of datasets more massive than currently available may provide the means to overcome this, but this eventuality is not guaranteed, particularly given the labor involved in manually annotating training images. We take a different tack, and instead leverage the massive amounts of data already residing in hospital picture archiving and communication systems (PACS) to develop a method to enhance CT images in a way that benefits lesion segmentation.

Fig. 1 presents some examples of current efforts at image enhancement. As Fig. 1(a) demonstrates, classic denoising methods, such as BM3D [6], can preserve image details while introducing very few artifacts. With the recent explosive development of deep convolutional neural networks (CNNs), the field has developed many CNN based denoising methods. These include DnCNN [7], which is able to handle denoising with unknown noise levels. However, most of the CNN based methods, including DnCNN [7], use mean squared error (MSE) loss for model optimization, which can blur high-frequency details, *e.g.* edges. See Fig. 1(c) for an example. Moreover, denoising methods do not explicitly address resolution and contrast issues.

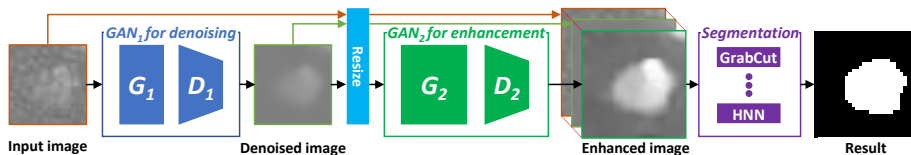


Fig. 2. The pipeline of the proposed method.

To overcome these problems, this paper proposes a novel CT image enhancement method by designing a stacked generative adversarial network (SGAN) model. As such, this work builds off of classic GANs [8], and is partially inspired by work using GANs for super resolution on natural images [9]. Unlike many natural images, CT images are often noisy and suffer from low contrast. Directly enhancing such images may generate undesirable visual artifacts and edges that are harmful for lesion segmentation accuracy. It is challenging to train a single GAN to directly output enhanced images with high resolution and visual quality from the original CT images. See Fig. 1(d) for the results produced by single GAN. One way to address this is to reduce CT image noise before image enhancement. Therefore, our proposed SGAN operates in two GAN stages. As shown in Fig. 1(e), the first GAN reduces the noise from the original CT image. As depicted in Fig. 1(f), the second GAN generates higher resolution images with enhanced boundary and contrast. Based on the enhanced images, the popular segmentation methods of GrabCut and holistically nested networks (HNNs) are used for lesion segmentation. Experimental results on the large scale DeepLesion dataset [10] demonstrate the effectiveness of our SGAN approach. In particular, we demonstrate that when using SGAN-enhanced with GrabCut, we can produce better results than the much more powerful, yet expensive, HNN applied to the original images, confirming our intuition on the value of attending to image quality.

## 2 Methods

Instead of directly performing image enhancement, our SGAN method decomposes enhancement into two sub-tasks, *i.e.*, image denoising followed by enhancement. After SGAN enhancement, either GrabCut or HNN is used for lesion segmentation. Figure 2 depicts the overall workflow of the proposed method. The details of each stage are described below.

### 2.1 CT Image Enhancement

In [9], generative adversarial networks (GANs) [8] were successfully used for natural-image super resolution, producing high-quality images with more visual details and edges compared to their low-resolution counterparts. For lesion segmentation, if we can improve visual clarity and contrast, particularly at the

borders of lesions, the segmentation performance and accuracy may subsequently be improved.

Given a CT lesion image (as shown in Fig. 1(a)), we first generate a denoised version of the input image by employing our first GAN model (consisting of a generator  $G_1$  and a discriminator  $D_1$ ) that focuses on removing random image noise. The denoised image has the same size as the input image. Although the noise has been reduced in the generated image, as demonstrated in Fig. 1(e), lesions have blurry edges and the contrast between lesion and background regions is generally low. As well, a considerable number of lesions are quite small in size ( $< 10\text{mm}$  or less than 10 pixels according to their long axis diameters). Human observers typically apply zooming (via commercial clinical PACS workstations) for such lesions. This motivates the use of a second GAN to provide high-resolution enhancement. To solve this issue, our second GAN model, which also contains a generator  $G_2$  and a discriminator  $D_2$ , is built upon the denoised image from the first GAN to produce an enhanced high resolution version (as illustrated in Fig. 1(f)). This enhanced high-resolution image provides both clear lesion boundaries and high contrast. Since the three resulting images, *i.e.*, the original, denoised, and enhanced variants, may have complementary information, we concatenate them together into a three-channel image that is fed into the next lesion segmentation stage.

**SGAN Architecture** We adapt similar architectures as [9] for the generators and discriminators, where the generator has 16 identical residual blocks and 2 sub-pixel convolutional layers [11], which are used to increase the resolution. Each block contains two convolutional layers with  $64\ 3 \times 3$  kernels followed by batch-normalization [12] and ParametricReLU [13] layers. Because it is an easier subtask, a simpler architecture that contains just 9 identical residual blocks is designed for the denoising generator  $G_1$ . As well, for a trained model, the method of [9] can only enlarge the input image by fixed amounts. However, in the DeepLesion dataset lesion sizes vary considerably, meaning they have to be enlarged with correspondingly different zooming factors. Therefore the sub-pixel layers are removed in the high-resolution generator  $G_2$ . Both  $G_1$  and  $G_2$  are fully convolutional and can take input images of arbitrary size. For the discriminator design,  $D_1$  and  $D_2$ , we use the same architecture as [9], which consists of 8 convolutional layers with  $3 \times 3$  kernels, LeakyReLU activations ( $\alpha = 0.2$ ), and two densely connected layers followed by a final sigmoid layer. The stride settings and kernel numbers of the 8 convolutional layers are (1, 2, 1, 2, 1, 2, 1, 2) and (64, 64, 128, 128, 256, 256, 512, 512), respectively.

**Training Data Synthesization** Normally super resolution models are trained with pairs of low- and high-resolution images. While this can be obtained easily in natural images (by down-sampling), physical CT images are imaged by medical scanners at roughly fixed in-plane resolutions of  $\sim 1\ \text{mm}$  per-pixel and CT imaging at ultra-high spatial resolutions does not exist. For the sake of SGAN training, we leverage transfer learning using a large-scale synthesized natural

image dataset: DIV2K [14] where all images are converted into gray scale and down-sampled to produce training pairs. For the training of the denoising GAN, we randomly crop  $32 \times 32$  sub-images from distinct training images of DIV2K. White Gaussian noise at different intensity variance levels  $\sigma_i \in (0, 50]$  are added to the cropped images to construct the paired model inputs. For training the image-enhancement GAN, the input images are cropped as  $128 \times 128$  patches and we perform the following steps: 1) down-sample the cropped image with scale  $s \in [1, 4]$ , 2) implement Gaussian spatial smoothing with  $\sigma_s \in (0, 3]$ , 3) execute contrast compression with rates of  $\kappa \in [1, 3]$ , and 4) conduct up-sampling with the scale  $s$  to generate images pairs. To fine-tune using CT images, we process 28,000 training RECIST slices using the currently trained SGAN and select a subset of up to 1,000 that demonstrate visual improvement. The selected CT images are subsequently added to the training for the next round of SGAN fine-tuning. This iterative process finishes when no more visual improvement can be observed.

**Model Optimization** A proper loss function needs to be defined for model optimization, which is critical for the performance of our generators. The generators are trained not only to generate high quality images but also to fool the discriminators. Similar to [9], given an input image,  $\mathbf{x}_i$  ( $i = 0, 1$ ), this work defines a perceptual loss  $L_P^i$  ( $i = 1, 2$ ) as the weighted sum of a image content loss  $L_C^i$ , a feature representation loss  $L_{VGG}^i$  and an adversarial loss  $L_A^i$  for  $G_1$  and  $G_2$  as

$$L_P^i = L_{DIFF}^i + 10^{-5}L_{VGG}^i + 10^{-3}L_A^i, \quad (1)$$

where  $i$  denotes the SGAN stage. Here,  $L_{DIFF}^i$  and  $L_{VGG}^i$  are computed using the mean square error (MSE) loss function to measure the pixel-wise error and the element-wise error of feature maps between the generated image  $G_i(\mathbf{x}_i)$  and its ground truth image  $\mathbf{y}_i$ , respectively. We extract feature maps from five blocks of the VGGNet-16 model [15] pre-trained over ImageNet [16]. The adversarial loss  $L_A^i$  is defined using the standard GAN formulation for generators:

$$L_A^i(\mathbf{x}_i) = -\log(D_i(G_i(\mathbf{x}_i))). \quad (2)$$

The discriminators, on the other hand, are trained to distinguish between real images and enhanced ones,  $\mathbf{y}_i$  and  $G_i(\mathbf{x}_i)$ , respectively, which can be accomplished by minimizing the following loss:

$$L_D^i(\mathbf{x}_i, \mathbf{y}_i) = -\log(D_i(\mathbf{y}_i)) - \log(1 - D_i(G_i(\mathbf{x}_i))) \quad (3)$$

We use the Adam optimizer [17] with  $\beta_1 = 0.5$  and a learning rate of  $10^{-4}$  for model optimization. The generator ( $G_1$  or  $G_2$ ) and discriminator ( $D_1$  or  $D_2$ ) are alternatively updated. We train first on the synthesized natural images and then fine-tune using the selected CT images.

## 2.2 Lesion Segmentation

Because they may contain complementary information, the denoised and enhanced outputs from the SGAN and the original lesion CT image are combined

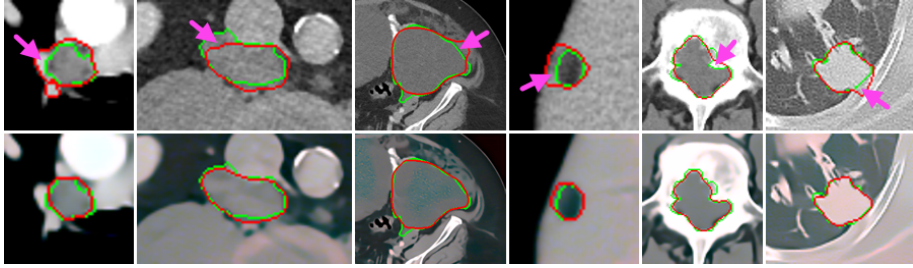


**Fig. 3.** Visual examples of lesion segmentation produced by HNN from the OG images (1<sup>st</sup> row) and their combinations with enhanced SGAN images (2<sup>nd</sup> row). The manual and automatic segmentation boundaries are delineated with green and red curves, respectively. Incorrectly segmented regions when using OG images that are corrected when using SGAN images are highlighted with pink arrows. Best viewed in color.

into a three-channel image for lesion segmentation. We investigate two popular segmentation approaches: GrabCut [18] and HNN [19]. The quality of GrabCut’s initialization will greatly affect the final segmentation result. For this reason, we construct a high quality *trimap*  $T$  using the RECIST diameter marks within the DeepLesion dataset [10]. This produces regions of probable background, probable foreground, background and foreground. Note that unlike the original *trimap* definition [18], we define four region types. With  $T$ , we can obtain the lesion segmentation using GrabCut. Since the DeepLesion dataset does not provide the ground truth lesion masks, the GrabCut segmentation results are used as supervision to train the HNN segmentation model until convergence.

### 3 Experimental Results and Analyses

The DeepLesion dataset [10] is composed of 32,735 PACS CT lesion images annotated with RECIST long and short diameters. These are derived from 10,594 studies of 4,459 patients. All lesions have been categorized into the 8 subtypes of lung, mediastinum, liver, soft-tissue, abdomen, kidney, pelvis, and bone. For quantitative evaluation, we manually segment 1,000 lesion images as a testing set, randomly selected from 500 patients. The rest serve as a training set. Based on the location of bookmarked diameters, CT region of interests (ROIs) are cropped at two times the extent of the lesion’s long diameters, so that sufficient visual context is preserved. Although we do not possess corresponding high quality images in the DeepLesion dataset, we can implicitly evaluate the performance of the proposed SGAN model for CT image enhancement by comparing the segmentation performance with or without enhanced images. Three criteria, *i.e.* Dice similarity coefficient (Dice), precision and recall scores, are used to evaluate the quantitative segmentation accuracy.

Figure 3 shows several visual examples of lesion segmentation results using HNN on original images and their combinations with the images produced by

**Table 1.** The performance of lesion segmentation using GrabCut and HNN with different inputs in terms of recall, precision and Dice score, whose mean and standard deviation are reported.

Input	GrabCut			HNN		
	Recall	Precision	Dice	Recall	Precision	Dice
OG	<b>0.944±0.096</b>	0.885±0.107	0.908±0.088	0.933±0.095	0.893±0.111	0.906±0.089
OG+BM3D	0.943±0.105	0.897±0.105	0.910±0.087	0.903±0.108	0.930±0.095	0.912±0.085
OG+DnCNN	0.944±0.101	0.892±0.108	0.909±0.090	0.901±0.114	0.927±0.098	0.910±0.086
OG+GAN	0.944±0.107	0.878±0.112	0.906±0.093	<b>0.937±0.109</b>	0.887±0.108	0.906±0.091
OG+GAN <sub>1</sub>	0.942±0.102	0.898±0.106	0.910±0.086	0.905±0.104	0.930±0.093	0.913±0.084
OG+SGAN	0.941±0.106	<b>0.904±0.096</b>	<b>0.913±0.085</b>	0.911±0.097	<b>0.940±0.091</b>	<b>0.920±0.082</b>

**Table 2.** Category-wise comparisons of lesion segmentation results using HNN on original images and their combinations with the images produced by SGAN. Mean and standard deviation of Dice score are reported.

Method	bone	abdomen	mediastinum	liver	
HNN	0.877±0.055	0.909±0.092	0.892±0.076	0.854±0.146	
SGAN+HNN	<b>0.891±0.061</b>	<b>0.927±0.088</b>	<b>0.909±0.083</b>	<b>0.877±0.142</b>	
Method	lung	kidney	soft tissue	pelvis	mDice
HNN	0.912±0.087	0.925±0.056	0.928±0.063	0.911±0.070	0.906±0.089
SGAN+HNN	<b>0.924±0.073</b>	<b>0.938±0.045</b>	<b>0.937±0.048</b>	<b>0.919±0.080</b>	<b>0.920±0.082</b>

SGAN. From Fig. 3, the segmentation results on the combined images are closer to the manual segmentations than the ones on only original images. This intuitively demonstrates that the enhanced images produced by the SGAN model is helpful for lesion segmentation.

For quantitative evaluation, we test both GrabCut and HNN applied on a variety of image options. Namely, we compare results when the original (OG) images are used, and also when those processed by BM3D [6], DnCNN [7]), a single GAN model (GAN) for enhancement, and the first denoising GAN model of SGAN (GAN<sub>1</sub>) are used. When enhancement is applied, we concatenate the result with OG images to create a multi-channel input for the segmentation method. From Table 1, we can see that 1) when using any of the enhanced images except the one produced by a single GAN, the Dice performance improves, supporting our intuition on the value of enhancing the CT images prior to segmentation. The possible reason of the worse results when using a single GAN is that it may enhance and introduce some artifacts. 2) Using GAN<sub>1</sub> for image denoising produces better Dice scores than using BM3D and DnCNN, suggesting that the adversarial learning strategy is helpful for image denoising while keeping details important for segmentation. 3) Compared with GrabCut, HNN achieves a greater improvement in Dice scores when using the enhanced images, suggesting HNN is able to exploit the complementary information better than GrabCut. 4) Using SGAN for image enhancement produces the largest gain in Dice scores. This confirms that our approach on using a stacked architecture can provide a more effective enhancement than just a blind application of GANs. 5) Most remarkably,

the Dice scores of GrabCut with SGAN is greater than just using HNN with OG images. Considering the simplicity of GrabCut, this indicates that focusing attention on improving data quality can sometimes yield larger gains than simply applying more powerful, but costly, segmentation methods. As a result, despite being somewhat neglected in the field, focusing attention on data enhancements can be an important means to push segmentation performance further.

Table 2 lists the Dice scores across lesion types when using HNN on OG and SGAN images. Notably, the segmentation performance over all categories is improved with SGAN images, with abdomen and liver exhibiting the largest improvement. These lesion categories may benefit the most due to their low contrast and blurred boundaries compared to the surrounding soft tissue.

## 4 Conclusions

We propose an SGAN method to enhance CT images to improve lesion segmentation performance. SGAN divides the task into two sub-tasks: the first GAN denoises the original CT image while the second generates a high quality image with higher resolution, enhanced boundaries, and higher contrast. Experimental results on the DeepLesion dataset test segmentation performance when GrabCut and HNN are applied on OG and enhanced images. Results demonstrate that SGAN is more effective than four other enhancement approaches, including using a single GAN, in yielding improved segmentation performance, with HNN + SGAN achieving the best performance. Most notably, Grabcut + SGAN outperformed HNN trained on the OG images, despite the latter having orders of magnitude more parameters. This demonstrates that focusing on dataset processing is a crucial research direction in medical imaging analysis.

**Acknowledgments.** This research was supported by the Intramural Research Program of the National Institutes of Health Clinical Center and by the Ping An Insurance Company through a Cooperative Research and Development Agreement. We thank Nvidia for GPU card donation.

## References

1. Tang, Y., Harrison, A.P., et al.: Semi-automatic recist labeling on ct scans with cascaded convolutional neural networks. arXiv:1806.09507 (2018)
2. Jin, D., Xu, Z., et al.: Ct-realistic lung nodule simulation from 3d conditional generative adversarial networks for robust lung segmentation. arXiv:1806.04051 (2018)
3. Cai, J., Tang, Y., et al.: Accurate weakly-supervised deep lesion segmentation using large-scale clinical annotations: Slice-propagated 3d mask generation from 2d recist. arXiv:1807.01172 (2018)
4. Massoptier, L., Casciaro, S.: A new fully automatic and robust algorithm for fast segmentation of liver tissue and tumors from ct scans. *European Radiology* **18**(8) (2008) 1658



5. Christ, P.F., Elshaer, M.E.A., et al.: Automatic liver and lesion segmentation in ct using cascaded fully convolutional neural networks and 3d conditional random fields. In: MICCAI. (2016) 415–423
6. Dabov, K., Foi, A., et al.: Image denoising by sparse 3-d transform-domain collaborative filtering. *IEEE TIP* **16**(8) (2007) 2080–2095
7. Zhang, K., Zuo, W., et al.: Beyond a gaussian denoiser: Residual learning of deep cnn for image denoising. *IEEE TIP* **26**(7) (2017) 3142–3155
8. Goodfellow, I., Pouget-Abadie, J., et al.: Generative adversarial nets. In: NIPS. (2014) 2672–2680
9. Ledig, C., Theis, L., et al.: Photo-realistic single image super-resolution using a generative adversarial network. In: CVPR. (2017) 4681–4690
10. Yan, K., Wang, X., et al.: Deep lesion graphs in the wild: relationship learning and organization of significant radiology image findings in a diverse large-scale lesion database. In: CVPR. (2018) 9261–9270
11. Shi, W., Caballero, J., et al.: Real-time single image and video super-resolution using an efficient sub-pixel convolutional neural network. In: CVPR. (2016) 1874–1883
12. Ioffe, S., Szegedy, C.: Batch normalization: Accelerating deep network training by reducing internal covariate shift. In: ICML. (2015) 448–456
13. He, K., Zhang, X., et al.: Delving deep into rectifiers: Surpassing human-level performance on imagenet classification. In: ICCV. (2015) 1026–1034
14. Agustsson, E., Timofte, R.: Ntire 2017 challenge on single image super-resolution: Dataset and study. In: CVPRW. (2017) 1122–1131
15. Simonyan, K., Zisserman, A.: Very deep convolutional networks for large-scale image recognition. *arXiv:1409.1556* (2014)
16. Deng, J., Dong, W., et al.: Imagenet: A large-scale hierarchical image database. In: CVPR. (2009) 248–255
17. Kingma, D.P., Ba, J.: Adam: A method for stochastic optimization. *arXiv:1412.6980* (2014)
18. Rother, C., Kolmogorov, V., et al.: Grabcut: Interactive foreground extraction using iterated graph cuts. In: ACM TOG. (2004) 309–314
19. Xie, S., Tu, Z.: Holistically-nested edge detection. In: ICCV. (2015) 1395–1403